Batteries & Supercaps

Research Article
doi.org/10.1002/batt.202400069

Chemistry Europe
European Chemical Societies Publishing

www.batteries-supercaps.org

Nonflammable Solid-State Polymer Electrolyte for High-Safety and Ultra-Stable Lithium-Ion Batteries

Chao Zhang,[a, b] Jingwen Liu,[a, b] Shenghao Zhang,[a, c] Minghui Wang,[b] Qingliang Lv,[a, c] Caixia Li,*[a, c] and Lei Wang*[a, b, c]

High safety and stability in batteries are crucial factors for the large-scale application of lithium-ion technology. In this work, flame-retardant aluminum diethylphosphonite (ADP) is coated by urea-formaldehyde (UF) shell to conquer the side reactions caused by ADP during cycling process. And then the core@shell structured ADP@UF is combined with poly(ethylene oxide) (PEO), high thermal stability can be realized. When exposed to high temperatures, ADP@UF generates N· and P· radicals to eliminate the combustion the H· and OH· radical, to inhibit fire. By controlling the percentage of flame retardant added, PEO-ADP@UF has totally achieved the effect of inflaming retarding, realizing stable electrochemical properties at the same time. The $-NH_2$ in UF forms hydrogen bonds with PEO, and acts as a Lewis base to promote the dissociation of lithium salts to increase the lithium-ion mobility number. Compared to PEO, battery with PEO-ADP@UF has outstanding cycling performance (103 mAh g^{-1} at 1 C, 2.5–4.2 V) and long service life (800 cycles).

1. Introduction

Polyethylene oxide (PEO) is one of the most representative materials in solid-state polymer electrolytes. PEO has received extensive attention in recent years owing to its advantages of high energy density, excellent flexibility, easy processing, and low cost.[1–3] However, there are also many obstructions to hinder its applications. Firstly, the excellent flexibility of PEO also means that its mechanical properties are poor, allowing lithium dendrites to grow at the anode during long cycling, easily penetrate the film and cause a short circuit.[4–5] Secondly, PEO-based electrolytes exhibit inherent disadvantages of low ion transfer ability.[6] Last but not least, PEO is flammable, which raises safety concerns during cycling.

Therefore, more and more researches focus on how to improve the electrochemical, mechanical and safety properties of PEO.[3] The incorporation of novel additives into PEO is an effective way to improve the safety performance, ionic conductivity (10^{-7}–10^{-6} S cm^{-1}), and electrochemical performance at room temperature.[7–8] Additives are generally categorized as organic and inorganic. Organics like β-cyclodextrin and butanedinitrile, etc., which increase the transfer rate of Li^+. However, the low melting point of organic molecules may reduce a reduction in the overall thermal stability of the polymer. Another strategy is to incorporate inorganic additives (SiO_2 or inorganic solid electrolyte powder, etc.) with PEO, which improve safety performance by building an organic-inorganic composite solid electrolyte (CSE) and inhibit the growth of lithium dendrites.[9–11] Unfortunately, the poor compatibility of inorganic materials with PEO makes it an obvious drawback, resulting in uneven distribution and low utilization rate which will affect the electrochemical performance and mechanical strength of CSE.

Therefore, suitable additives with flame retardancy to combine with PEO will improve the thermal stability and electrochemical performance of the battery.[12–13] The aluminum diethylphosphinate (ADP) is a kind of halogen-free flame retardant which is eco-friendly. It also has superior flame-retardant efficiency because of high phosphorus content. Therefore, ADP is widely applied in polymer fabrication with high flame retardant efficiency.[14–16] The concern is that the direct addition of flame retardants negatively affects the electrochemical performance of SPE. During charge-discharge process, the small molecules or functional groups in flame retardant are directly involved in the electrochemical reaction, and the generated by-products seriously impede the cycling performance.[16–17] In order to further improve cycling stability, microcapsule technology is adopted by coating the flame retardant to avoid side reactions.[18–20]

In this work, we encapsulate ADP with urea-formaldehyde (UF) to prepare microcapsule (ADP@UF). The UF resin is suitable for protecting ADP because of high structural stability. The flame retardant SPE (PEO-ADP@UF) is obtained by incorporating ADP@UF into PEO. The $-NH_2$ carried by UF forms a continuous hydrogen bonding network with the –O– in PEO, which improves the mechanical strength, inhibits the growth of lithium dendrites, and extends the cycle life of the battery. On

[a] C. Zhang, J. Liu, S. Zhang, Q. Lv, Prof. C. Li, Prof. L. Wang
State Key Laboratory Base of Eco-Chemical Engineering, International Science and Technology Cooperation Base of Eco-chemical Engineering and Green Manufacturing, Qingdao University of Science and Technology, Qingdao 266042, P. R. China
E-mail: licaixia91@126.com
inorchemwl@126.com

[b] C. Zhang, J. Liu, Prof. M. Wang, Prof. L. Wang
College of Chemistry and Molecular Engineering, Qingdao University of Science and Technology, Qingdao 266042, P. R. China

[c] S. Zhang, Q. Lv, Prof. C. Li, Prof. L. Wang
Shandong Engineering Research Center for Marine Environment Corrosion and Safety Protection, College of Environment and Safety Engineering, Qingdao University of Science and Technology, Qingdao, 266042, China

Supporting information for this article is available on the WWW under https://doi.org/10.1002/batt.202400069

Research Article
doi.org/10.1002/batt.202400069
Chemistry Europe
European Chemical Societies Publishing

the other hand, –NH_2 increases the Lewis alkalinity of SPE and promotes the ability of the PEO unit to dissociate the lithium salt. It is worth noting that the ADP@UF produces P· and N· to capture radicals (OH·, H·), slowing down the rate of combustion when the temperature rise. Further combustion will form a protective layer of NO, NO_2 and H_3PO_4, preventing the combustion.[21–24] The LOI value of PEO-ADP@UF is 27% verifying the flame-retardant effect. In addition, the Li symmetric battery maintains ultra-stable Li^+ plating/stripping for more than 1000 h at 0.1 mA cm^{-2}. After 800 cycles at 1 C, the LFP//Li battery exhibits excellent cycling stability and high capacity of 103.5 mAh g^{-1}.

2. Results and Discussion

Microcapsules (ADP@UF) are prepared by microencapsulation technology, in which urea-formaldehyde resin (UF) coated on the flame retardant (ADP). Then ADP@UF is doped into the PEO, and finally the flame-retardant solid polymer electrolyte (PEO-ADP@UF) is formed, as shown in the Scheme 1a. Thanks to the presence of UF, ADP is stable in SPE without decomposition. During the process of in-situ polymerization, the flame-retardant surface activity is increased by the emulsification of the emulsifier, which allows UF to polymerize around ADP very smoothly.[24] During the charging process of the full battery with PEO-ADP@UF, Li^+ moves to the cathode (Scheme 1b). At high temperatures, the ADP@UF in PEO-ADP@UF exerts superlative flame-retardant effect, as show in the Scheme 1c. ADP and UF decompose to produce radicals (P· and N·) that capture hydroxyl radical (OH·), hydrogen radical (H·), slowing down the combustion. The combustion products generate a protective layer with NO, NO_2 and H_3PO_4 on the surface of the polymer at high temperatures. As the temperature rises, this could trigger carbonization by generating a stable carbon layer, which blocks heat conduction and oxygen diffusion and prevents the combustion reaction.[16] The synergistic effect of N and P elements and carbon layer create a gas-solid double protective layer, which greatly improves the safety performance of PEO-ADP@UF.

To verify the structure of ADP@UF, the surface morphology and elemental composition of microencapsulations are investigated by TEM and SEM observations. As shown in Figure 1a–b, the surface of the microencapsulations is relatively flat with diameters are about 1–3 μm, without agglomeration and uniformly dispersed. As shown in Figure 1c, the EDS spectrum of ADP@UF, the content of O is the most and the content of Al is almost absent. Figure 1d shows the elemental mapping image of ADP@UF, which distinguishes the distribution of C, O, N, P, and Al elements by different colors.[20] It should be noted that the Al has not been detected indicating the packaging by UF, and the PEO-ADP@UF is successfully designed. Figure S1 shows the FT-IR spectra of powder ADP and PEO. Due to the stretching of –CH_2– and C–O–C, peaks can be found in the spectrum of PEO at 957 cm^{-1} and 1100 cm^{-1}. The visible peaks at 1340 cm^{-1} and 1460 cm^{-1} are owing to the shearing effect of –CH_3. The characteristic peak P–C of ADP is located at 780 cm^{-1}. The peak values of 1070 cm^{-1} and 1150 cm^{-1} are caused by stretching vibrations of the P–O and P=O.[25]

PEO-ADP@UF is prepared by a casting process containing the ADP. As shown in Figure S2a–b, d–e, g–h, the surface smoothness of PEO-ADP@UF remains the same as that of PEO, but the addition of ADP increases the roughness of the PEO-ADP surface with significant void generation. In addition to the smooth and flat surface of the SPE, its tight cross-section also plays an important role in influencing the interfacial impedance of the battery. For comparison, the cross-section of PEO-ADP@UF is tighter than PEO and PEO-ADP, as shown in Figure S2c,f,i. The results of SEM indicates that PEO-ADP@UF has a smooth and flat surface and a dense interior in terms of the morphology of the SPE, which provides adequate contact between electrolyte with the electrode.[26] As shown in Figure 2a, the characteristic peak values of –CH_2– and C–O–C in PEO-ADP@UF are 960 cm^{-1} and 1100 cm^{-1}, respectively. The characteristic peaks of –CH_2– and C–O–C from PEO are present in the three samples. Unusually, PEO-ADP has three extra characteristic peaks from ADP, where the characteristic peaks of 788 cm^{-1}, 1070 cm^{-1} and 1145 cm^{-1} correspond to P–C, P–O and P=O, respectively.[25] Therefore, ADP has been coated by UF and PEO-ADP@UF is synthesized successfully. As shown in Figure 2b, the X-ray diffraction spectra (XRD) of PEO-ADP@UF is consistent with that of PEO. The diffraction peaks located at 19° and 23.2° are presented in all samples simultaneously and the peak heights in PEO-ADP@UF and PEO-ADP significantly reduce,

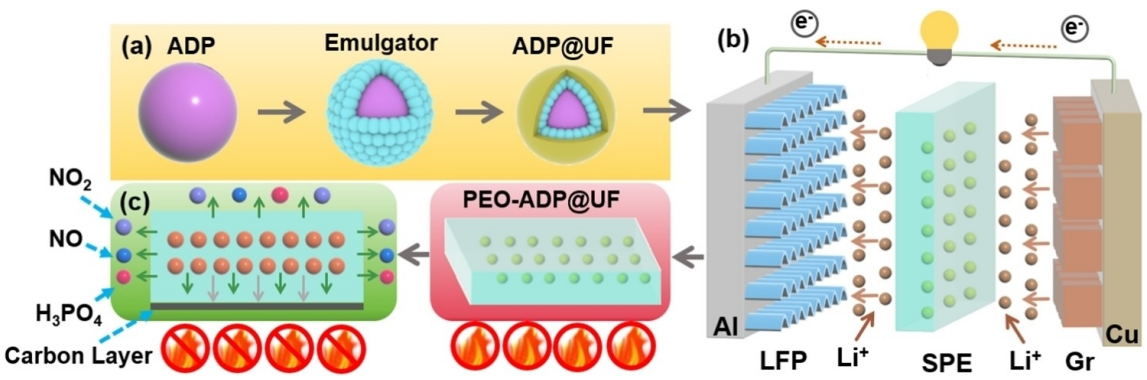

Scheme 1. (a) Synthesis of ADP@UF, (b) application of PEO-ADP@UF in LFP//Gr battery at discharging state and (c) its flame-retardant effect during cycling.

Research Article
doi.org/10.1002/batt.202400069
Chemistry Europe
European Chemical Societies Publishing

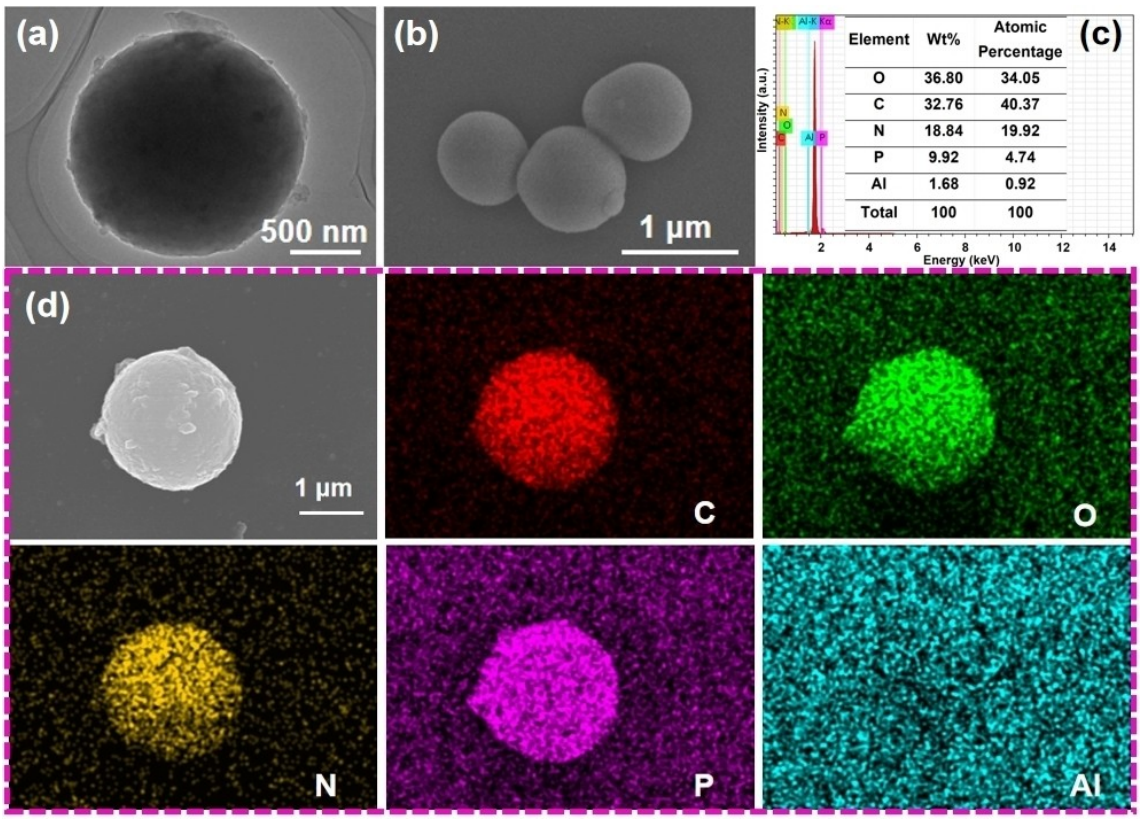

Figure 1. (a) TEM images and (b) SEM images of ADP@UF. (c) The EDS spectrum of ADP@UF. (d) SEM images and corresponding mapping images of C, O, N, P and Al for ADP@UF.

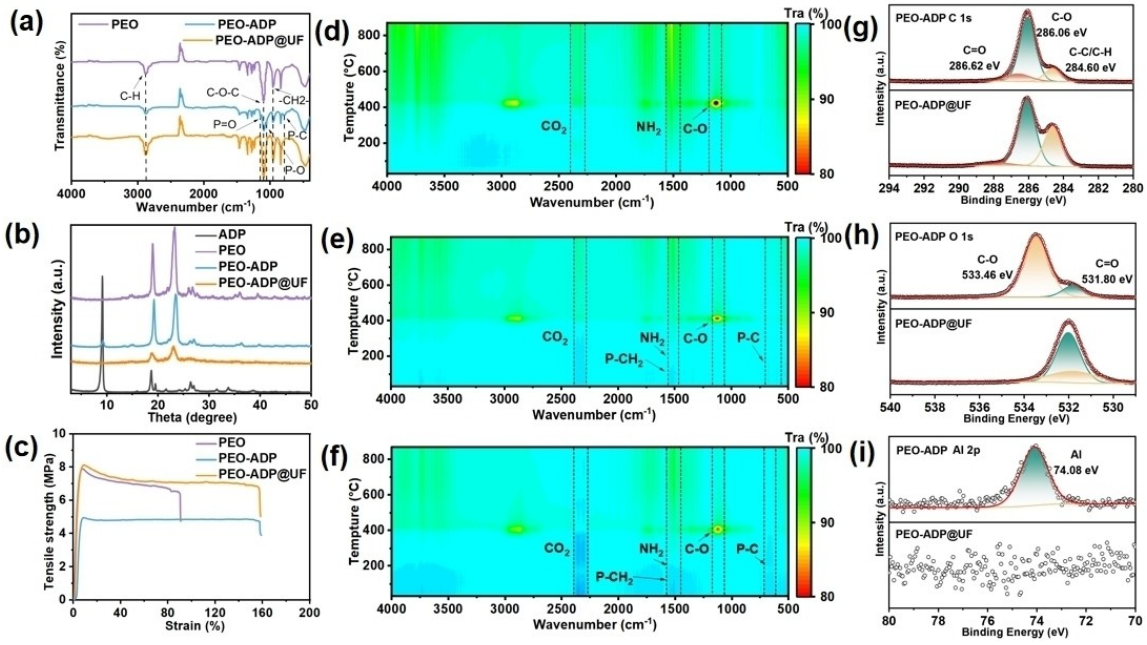

Figure 2. (a) FTIR curves of PEO, PEO-ADP and PEO-ADP@UF. (b) XRD curves of ADP, PEO, PEO-ADP and PEO-ADP@UF. (c) Stress-strain curves of PEO, PEO-ADP and PEO-ADP@UF. (d–f) The FTIR of in-situ TG-IR heatmap of PEO, PEO-ADP and PEO-ADP@UF. (g–i) XPS spectra of PEO-ADP and PEO-ADP@UF of (g) C 1s, (h) O 1s and (i) Al.

which suggests the addition of ADP and ADP@UF can reduce the crystallinity of the polymers and favor the migration of Li^+ in SPE.[27–28] Besides, the addition of ADP@UF plays a role in the flexibility of the material. As shown in Figure 2c, with 25% ADP,

Research Article
doi.org/10.1002/batt.202400069
Chemistry Europe
European Chemical Societies Publishing

the maximum value of PEO-ADP's tolerable pressure is 5 MPa.[11] PEO-ADP@UF increases the film's elongation to 156%, and enhances the withstanding pressure to 6 MPa. The $-NH_2$ of ADP@UF forms hydrogen bonds with the O of the matrix PEO, which builds interconnected networks and improves mechanical strength of SPE.[29] The improvement of mechanical strength means that the ability of SPE to inhibit lithium dendrite growth is also improved. To analyze the changes in the thermal decomposition, the thermogravimetric-infrared hyphenation (TG-IR) is performed. As shown in Figure 2f, PEO-ADP@UF decomposes slowly in the range of less than 400 °C at a heating rate of 10 °C min^{-1}. The peaks in the 600–700 cm^{-1} range belong to P–C and those in 1440–1580 cm^{-1} are caused by the stretching deformation of the C–H bond in P–CH_2 and the bending vibration of the N–H bond in $-NH_2$.[16] However, the intensities of the characteristic peaks of P–C and P–CH_2 in PEO-ADP are significantly weaker (Figure 2e). The characteristic peak of the C–O bond as the matrix PEO consistently appeared in all three samples (Figure 2d).[30] As shown in Figure S3a–c, PEO-ADP@UF and PEO-ADP are decomposed by heating, and the mass percentage of carbon residue are 7.5% and 14.7%, which indicates that the addition of ADP@UF and ADP improves the thermal stability of PEO. Although the same mass of ADP and ADP@UF is added, more carbon residue is formed after thermal decomposition of PEO-ADP@UF. This indicates that ADP@UF prefers to form a carbon layer to prevent combustion under thermal runaway, while UF prefers to form a gaseous protective layer.

The chemical interactions of ADP and ADP@UF incorporated into PEO are evaluated by x-ray photoelectron spectroscopy (XPS). In the C1s spectrum (Figure S4a), the C–O peak of PEO is located at 286.00 eV. After the addition of flame retardant, the binding energy C–O of PEO-ADP and PEO-ADP@UF are 286.06 eV and 286.11 eV, respectively.[31–33] However, in the corresponding O 1s spectrum, the binding energy value of C–O in PEO-ADP@UF at 532.02 eV is lower than that of PEO and PEO-ADP, as shown in Figure 2h,S4b. Since the doping of ADP@UF, $-NH_2$ acts as a Lewis base to provide electrons to form lone electron pairs with O in PEO resulting in Lewis addition products, which leads to a smaller peak of C–O than that of PEO. It is noteworthy that a separate peak belongs to the aluminum hydroxide ($Al(OH)_3$) for PEO-ADP in the Al 2p spectrum with a binding energy of 74.08 eV, while no peak is formed for PEO-ADP@UF, as shown in Figure 2i.[25] This shows that ADP is completely encapsulated by UF and effectively prevents the leakage of ADP through microencapsulations.

The thermal stability of SPE is being investigated. The heating test method is applied, which maintains at 30 °C, 60 °C, 90 °C, 120 °C, and 150 °C for 30 min. As shown in Figure 3a, PEO can be stable at 60 °C, but starts to curl at 90 °C. In contrast, PEO-ADP@UF and PEO-ADP show no abnormal changes such as curling from the beginning heating of 30 °C to 150 °C. This proves that both ADP and ADP@UF improve the degree of heat

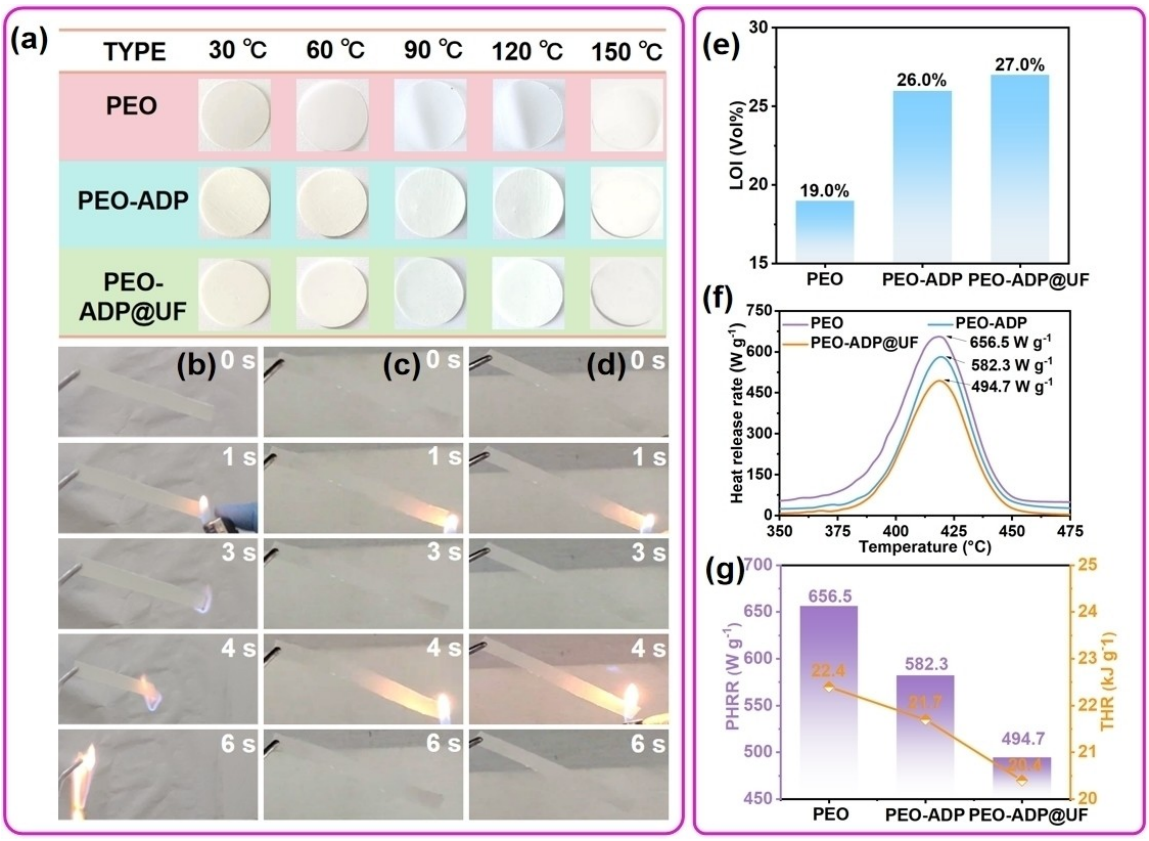

Figure 3. (a) Thermal contraction film, (b–d) ignition test, (e) Limiting oxygen index (LOI) values, (f) heat release rate curves, and (g) heat release rate (HRR) and total heat release (THR) of PEO, PEO-ADP and PEO-ADP@UF.

Research Article
doi.org/10.1002/batt.202400069
Chemistry Europe
European Chemical Societies Publishing

resistance of PEO. When the PEO is ignited, flame remains 6 s (Figure 3b). As shown in Figure S5a–c, the amount of ADP added gradually increased from 5%, 10% and 15% the burning time is also gradually up to 11 s, 16 s and 21 s. In Figure S5d, with the content of 20% ADP, the surface of the material is carbonized after the burning for 7 s.[21,33–34] As shown in Figure 3c,d, the content of ADP and ADP@UF is increased to 25% and the flame could not ignite the films. The results prove that high levels of ADP and ADP@UF can effectively improve the flame-retardant performance of PEO. As shown in Figure 3d, the LOI value for PEO is 19%, and PEO-ADP and PEO-ADP@UF reach 26% and 27%, respectively.[13,35] In addition, microscale calorimeter (MCC) is applied to assess the resistance to fire risk of SPE. As shown in Figure 3e, the heat release rate (HRR) values of PEO-ADP@UF is much lower than PEO and PEO-ADP. This indicates that ADP@UF effectively reduces the heat released during the combustion process of the PEO matrix, which leads to the HRR of PEO-ADP@UF decreasing to 161.7 $W g^{-1}$.[21] The HRR of SPE simultaneously affects the total heat release (THR) values, as shown in Figure 3f. This shows that ADP@UF as a novel flame retardant effectively slows down the exothermic rate during the combustion of PEO. During combustion, ADP decomposes a protective layer of $Al(OH)_3$ to acts as an air barrier, which inhibits the combustion. The P· and N· generated by ADP@UF eliminate O· and OH·, interrupting the spontaneous combustion reaction. The carbon layer isolates oxygen diffusion and heat transfer, preventing further combustion reactions.

The conductivities of PEO, PEO-ADP and PEO-ADP@UF are obtained from electrochemical impedance spectra (EIS). As shown in Figure 4a, we use stainless steel (SS) as an electrode to test the impedance maps of SPE, in which the ion conductivities of PEO, PEO-ADP and PEO-ADP@UF are 1.05×10^{-3} S cm^{-1}, 1.05×10^{-3} S cm^{-1} and 1.74×10^{-3} S cm^{-1}.[36] In Li symmetric batteries, the impedance value of PEO-ADP@UF remained minimal with an ionic conductivity of 1.50×10^{-4} S cm^{-1} (Figure 4b). The excellent interfacial contact of PEO-ADP@UF facilitates the impedance value to remain consistently low, not only in Li symmetric battery but also in LFP battery (Figure 4c). The stable electrochemical window of the SPE, is shown in Figure 4d. In the symmetric battery composed of SS, the voltage window of PEO and PEO-ADP@UF are 4.7 V and the voltage window of PEO-ADP is 4.5 V.[28] In LFP//Li battery, due to the presence of ADP, the PEO-ADP voltage window is 4.7 V, which is less than the value of 5 V for PEO-ADP@UF (Figure 4e). Based on the Nyquist plots of the studied SPEs at 30–70 °C, the ionic conductivity (σ) of PEO-ADP@UF is calculated to be much larger than that of PEO-ADP, as shown in Figure S6a–c.[36–37] By the Arrhenius formula, the activation energy (E_a) can be calculated, where PEO, PEO-ADP, and PEO-ADP@UF are 0.27 eV, 0.44 eV, and 0.24 eV respectively, as

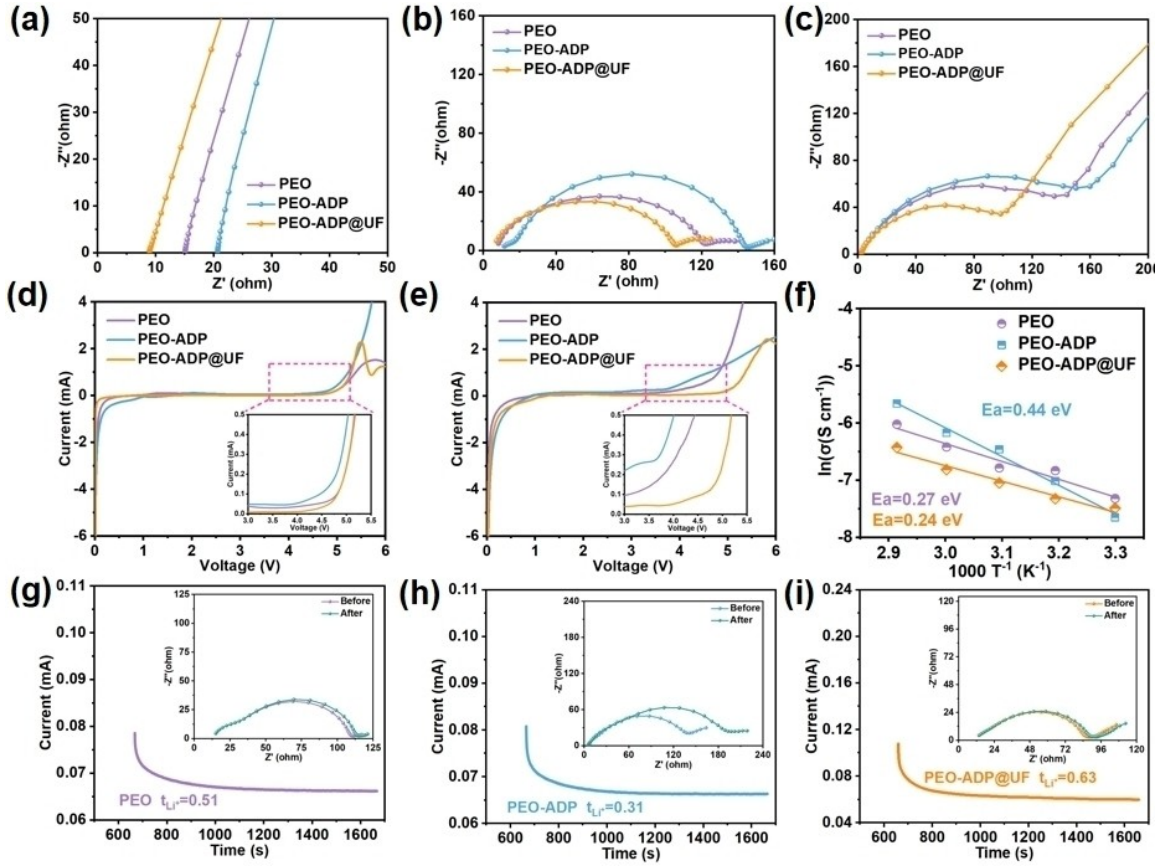

Figure 4. (a) EIS curves with SS//Li, (b) LFP//Li//Li and (c) LFP//Li. (d) LSV curves with SS//Li and (e) LFP//Li. (f) The temperature dependence of the ionic conductivities and corresponding fitting results according to the Arrhenius formula. (g–i) Chronoamperometry profiles of Li//Li batteries.

Research Article
doi.org/10.1002/batt.202400069
Chemistry Europe
European Chemical Societies Publishing

shown in Figure 4f.[13,38–39] This demonstrates that the ion migration

barrier in PEO-ADP@UF is the smallest. The –NH_2 in ADP@UF acts as a Lewis base to promote the dissociation of lithium salts and modulate the chemical environment of Li^+, which leads to an increase in ionic conductivity and a decrease in the ionic mobility barrier. In addition to ionic conductivity and electrochemical window, Li^+ transfer number is also one of the important parameters for battery performance. Compared with PEO-ADP (0.31), PEO-ADP@UF and PEO are equipped with the Li^+ transfer number of 0.63 and 0.51.[40] The Li^+ in PEO are constantly jumping between ether-oxygen bonds.[16,41] The enhancement of Li^+ transfer number of PEO-ADP@UF is attributed to the coordination of –NH_2 with O in the matrix PEO, which reduces the coordination capacity of Li–O and improves the rate of Li^+ migration.

As shown in Figure 5a, at a current density of 0.1 mA cm^{-2}, the polarization voltage of PEO is the largest among the three materials, with an overpotential of about 100 mV. The overpotential of PEO-ADP enhanced within 100 h, indicating that the lithium deposition at the interface is not homogeneous and hinders the migration of Li^+. PEO-ADP@UF starts with a low overpotential value of 65 mV and cycles stably for over 1000 h. As shown in Figure 5b, the overpotential of PEO-ADP@UF at 750 h is 200 mV, which is less than 238 mV for PEO and 275 mV for PEO-ADP at 0.3 mA cm^{-2}. In addition, the overpotential and life-span of PEO-ADP@UF at 0.5 mA cm^{-2} are also superior than others (Figure 5c). With cycling, the lithium dendrites in the battery grow irreversibly, which leads to the battery failing.[42] The PEO-ADP@UF improve the ion transfer number and mechanical properties, which inhibits lithium dendrites and improves the stable plating/stripping behavior of symmetric batteries.

To evaluate the ability of different types of SPEs to inhibit lithium dendrites, exploring the maximum current density of Li symmetric battery cycling (critical current density, CCD) is performed. During cycling, the current density increases by 0.05 mA cm^{-2} every 30 minutes.[43] As shown in Figure 5f, CCD of PEO-ADP@UF reaches a maximum value of 1.50 mA cm^{-2}. As shown in Figure 5d–e, the CCD values for PEO and PEO-ADP are 1.45 mA cm^{-2} and 1 mA cm^{-2}, respectively.[44] Due to high electronic conductivity, PEO-ADP@UF improves the transfer of Li^+, and prevents Li^+ from accumulating at the interface. In summary, the synergistic effect of high ionic conductivity and high mechanical strength brought by ADP@UF greatly improves the applicability of PEO-ADP@UF in Li symmetric battery. In situ FT-IR is applied to test the stability of SPE during the charging/discharging process of Li symmetric battery. As for PEO-ADP, the characteristic peak change of 420–560 cm^{-1} belongs to P–C.[45–46] Due to the influence of electrochemical reactions, the value of the P–C characteristic peak originally located at 780 cm^{-1} decreased, and the peak intensity changed significantly during the transition from charging to discharging. This originates from the decomposition products of ADP during charging/discharging, as shown in Figure 5h. As shown in Figure 5g, i, the characteristic peaks in the range of 650–1070 cm^{-1} belong to C–O–C and –CH_2–, which indicates the functional group changes on the SPE surface are mainly from the PEO matrix.

Electrochemical performance of LFP//Li with PEO-ADP@UF, PEO-ADP and PEO SPE is investigated. As shown in Figure 6a, PEO-ADP@UF reaches the specific capacity of 150 mAh g^{-1} at the 21st after initial stabilization. After 800 cycles, the specific capacity still maintains a high value of 110 mAh g^{-1} (Figure S7c).[26,38,47] As shown in Figure 6b, with the current density of 1 C, PEO-ADP@UF still maintains excellent cycling performance. Without the addition of ADP@UF, the PEO shows a significant downward trend after 400 cycles of stable cycling at 0.5 C, which leads to its final initial capacity retention of 50%. PEO-ADP@UF reaches the specific capacity of 92.19 mAh g^{-1} after 600 cycles of stable cycling at 2 C, as shown in Figure 6c. As shown in Figure S7a–b,d–e, as for the poor cycling performance of PEO-ADP, it is attributed to the decomposition of ADP during the electrochemical reaction of SPE, which leads to the

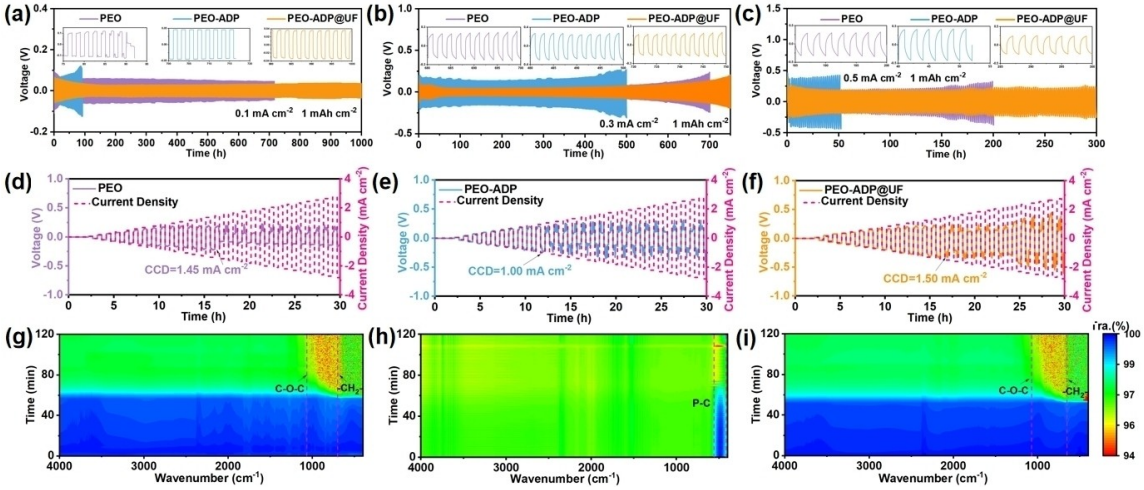

Figure 5. (a–c) voltage profiles of Li//Li batteries at 0.1 mA cm^{-2}, 0.3 mA cm^{-2} and 0.5 mA cm^{-2}, (d–f) critical current density (CCD) measurement of Li//Li batteries with PEO, PEO-ADP and PEO-ADP@UF. In situ FTIR spectra curves (g) PEO, (h) PEO-ADP and (i) PEO-ADP@UF during Li//Li batteries discharging and charging process.

Research Article
doi.org/10.1002/batt.202400069
Chemistry Europe
European Chemical Societies Publishing

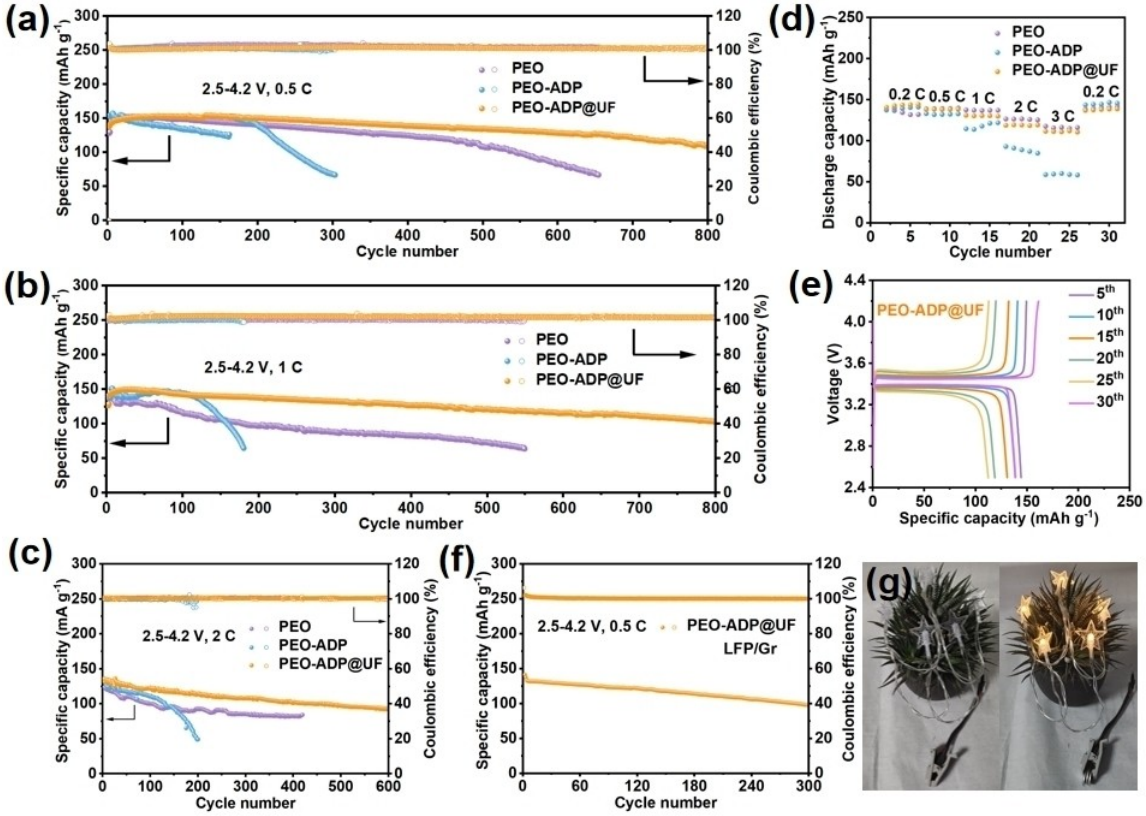

Figure 6. (a) Cycle performance of LFP//Li batteries at a voltage range of 2.5–4.2 V at 0.5 C with PEO, PEO-ADP and PEO-ADP@UF, (b) at 1 C and (c) at 2 C. (d) Rate performance of LFP//Li batteries, and corresponding voltage profiles of (e) PEO-ADP@UF. (f) Cycle performance of LFP//Gr batteries with PEO-ADP@UF at a voltage range of 2.5–4.2 V at 0.5 C. (g) Demonstration picture of lighting LED lamps.

accumulation of by-products on the anode surface to produce a thicker SEI layer, and seriously hampers the delivery of Li^+. The PEO-ADP@UF still able to cycle steadily for 600 cycles at 2 C. It is worth noting that the cyclic performance of PEO-ADP@UF is better than PEO and PEO-ADP, as shown in Figure S7f. Multiplier performance is further explored through the variation of the specific capacity of SPE at different currents. As shown in Figure 6d, the PEO-ADP@UF corresponding specific capacities are 144.4, 138.6, 130, 125.5, 110.7 and 138.9 mAh g^{-1} at currents of 0.2, 0.5, 1, 2, 3, and 2 C. The specific capacity of PEO-ADP@UF is relatively stable with PEO cycling cycles, but PEO-ADP shows a severe decline in specific capacity at 1 C, 2 C and 3 C corresponding to 122.1 mAh g^{-1}, 85 mAh g^{-1} and 58.4 mAh g^{-1}. Figure 6e shows the charge/discharge curve of PEO-ADP@UF, which corresponds to the multiplicity performance and the specific capacity of 138.7 mAh g^{-1} after a current return to 0.1 C. This indicates that the PEO-ADP@UF is more practical in the future with the greater range of withstand currents. To investigate the commercial value of SPE electrolytes, graphite (Gr) battery is assembled (Figure 6f). The Li battery with PEO-ADP@UF SPE is successfully light LEDs demonstrating practical applications.

3. Conclusions

This work has prepared ADP@UF by in situ polymerisation of UF on the surface of ADP using microcapsule encapsulation to solve the side-reactions of flame-retardant for lithium batteries. The $-NH_2$ group in ADP@UF functions as the Lewis base, offering electron pairs that facilitates the dissociation of lithium salts and promotes the migration of Li^+. In addition, $-NH_2$ forms hydrogen bonds with the ether oxygen bonds in PEO, which would weaken the bonding energy of Li–O and increase the Li^+ migration. PEO-ADP@UF has a high LOI value of 27%, which improve the safety of lithium battery greatly. Battery with PEO-ADP@UF exhibits high specific capacity at 0.5 C, 1 C and 2 C.

Acknowledgements

This work was supported by the National Natural Science Foundation of China (52202260, 52272222, 22002083 and 52072197), the Natural Science Foundation of Shandong Province (ZR2021QE037), University Youth Innovation Team of Shandong Province (202201010318), Taishan Scholar Young Talent Program (tsqn202306219, tsqn201909114), Outstanding Youth Foundation of Shandong Province, China (ZR2019JQ14), Shandong Province Double-Hundred Talent Plan (WST2020003).

Conflict of Interests

The authors declare no conflict of interest

Data Availability Statement

The data that support the findings of this study are available in the supplementary material of this article.

Keywords: polymer electrolyte · nonflammable · Lewis base · high safety · lithium battery

[1] X. Yu, Z. J. Hoffman, J. Lee, C. Fang, L. A. Gido, V. Patel, H. B. Eitouni, R. Wang, N. P. Balsara, *ACS Energy Lett.* **2022**, *7*, 3791–3797.
[2] Z. Zhang, YingHuang, G. Zhang, L. Chao, *Energy Storage Mater.* **2021**, *41*, 631–641.
[3] H. Duan, L. Li, K. Zou, Y. Deng, G. Chen, *ACS Appl. Mater. Interfaces* **2021**, *13*, 57380–57391.
[4] S. Liu, W. Liu, D. Ba, Y. Zhao, Y. Ye, Y. Li, J. Liu, *Adv. Mater.* **2022**, *35*, 2110423.
[5] Z. Xiong, Z. Wang, W. Zhou, Q. Liu, J.-F. Wu, T.-H. Liu, C. Xu, J. Liu, *Energy Storage Mater.* **2023**, *57*, 171–179.
[6] T. T. Vu, H. J. Cheon, S. Y. Shin, G. Jeong, E. Wi, M. Chang, *Energy Storage Mater.* **2023**, *61*, 102876.
[7] C. Liu, F. Zhu, Z. Huang, W. Liao, X. Guan, Y. Li, D. Chen, Z. Lu, *Chem. Eng. J.* **2022**, *434*, 134644.
[8] M. J. Lee, J. Han, K. Lee, Y. J. Lee, B. G. Kim, K.-N. Jung, B. J. Kim, S. W. Lee, *Nature* **2022**, *601*, 217–222.
[9] J. Ma, G. Zhong, P. Shi, Y. Wei, K. Li, L. Chen, X. Hao, Q. Li, K. Yang, C. Wang, W. Lv, Q.-H. Yang, Y.-B. He, F. Kang, *Energy Environ. Sci.* **2022**, *15*, 1503–1511.
[10] J. Wen, Q. Zhao, X. Jiang, G. Ji, R. Wang, G. Lu, J. Long, N. Hu, C. Xu, *ACS Appl. Energ. Mater.* **2021**, *4*, 3660–3669.
[11] C. Wang, T. Yang, W. Zhang, H. Huang, Y. Gan, Y. Xia, X. He, J. Zhang, *J. Mater. Chem. A* **2022**, *10*, 3400–3408.
[12] L. Liu, M. Zhu, Z. Ma, X. Xu, J. Dai, Y. Yu, S. Mohsen Seraji, H. Wang, P. Song, *Chem. Eng. J.* **2022**, *440*, 135645.
[13] M.-C. Long, G. Wu, X.-L. Wang, Y.-Z. Wang, *Energy Storage Mater.* **2022**, *53*, 62–71.
[14] Q. Wang, L. Jiang, Y. Yu, J. Sun, *Nano Energy* **2019**, *55*, 93–114.
[15] T. M. Nguyen-Ha, T. B. Nguyen, T. A. Nguyen, L. H. Pham, D. H. Nguyen, D. M. Nguyen, D. Hoang, E. Oh, J. Suhr, *Chem. Eng. J.* **2023**, *474*, 145585.
[16] L. Han, C. Liao, X. Mu, N. Wu, Z. Xu, J. Wang, L. Song, Y. Kan, Y. Hu, *Nano Lett.* **2021**, *21*, 4447–4453.
[17] Y. Yin, Y. Yang, D. Cheng, M. Mayer, J. Holoubek, W. Li, G. Raghavendran, A. Liu, B. Lu, D. M. Davies, Z. Chen, O. Borodin, Y. S. Meng, *Naure Energy* **2022**, *7*, 548–559.
[18] Y. Wu, J. Long, B. Liang, Y. Yanan, *Pigm. Resin Technol.* **2022**, *53*, 62–68.
[19] C. Zotiadis, I. Patrikalos, V. Loukaidou, D. M. Korres, A. Karantonis, S. Vouyiouka, *Prog. Org. Coat.* **2021**, *161*, 106475.
[20] Y. Roh, D. Kim, D. Jin, D. Kim, C. Han, J. Choi, H. Lee, Y.-G. Lee, Y. M. Lee, *Chem. Eng. J.* **2023**, *474*, 145937.
[21] J. Xie, S. Qiao, Y. Wang, J. Sui, L. Bao, H. Zhou, T. Li, J. Wang, *J. Energy Chem.* **2023**, *80*, 324–334.
[22] T. Zhu, G. Liu, D. Chen, J. Chen, P. Qi, J. Sun, X. Gu, S. Zhang, *Energy Storage Mater.* **2022**, *50*, 495–504.
[23] H. Y. Zhou, S. S. Yan, J. Li, H. Dong, P. Zhou, L. Wan, X. X. Chen, W. L. Zhang, Y. C. Xia, P. C. Wang, B. G. Wang, K. Liu, *ACS Appl. Mater. Interfaces* **2022**, *14*, 24469–24479.
[24] Q. Liu, T. Yu, H. Yang, S. Xu, H. Li, K. Chen, R. Xu, T. Zhou, Z. Sun, F. Li, *Nano Energy* **2022**, *103*, 107763.
[25] Y. Wang, J. Yuan, L. Ma, X. Yin, Z. Zhu, P. Song, *Carbohydr. Polym.* **2022**, *298*, 120141.
[26] Y. Hou, Z. Huang, Z. Chen, X. Li, A. Chen, P. Li, Y. Wang, C. Zhi, *Nano Energy* **2022**, *97*, 107204.
[27] N. Lv, Q. Zhang, Y. Xu, H. Li, Z. Wei, Z. Tao, Y. Wang, H. Tang, *J. Alloys Compd.* **2023**, *938*, 168675.
[28] M. Li, K. Wang, J. Liu, F. Shen, C. Xu, X. Han, *J. Colloid Interface Sci.* **2022**, *622*, 1029–1036.
[29] F. Chen, C. Guo, H. Zhou, M. W. Shahzad, T. X. Liu, S. Oleksandr, J. Sun, S. Dai, B. B. Xu, *Small* **2022**, *18*, 2106352.
[30] G. Jiang, X. Xu, J. Zhang, C. He, S. Tao, Y. Wu, Y. Ding, *J. Anal. Appl. Pyrolysis* **2024**, *177*, 106306.
[31] M.-C. Long, P.-H. Duan, Y. Gao, X.-L. Wang, G. Wu, Y.-Z. Wang, *Chem. Eng. J.* **2022**, *432*, 134394.
[32] W. Liu, G. Li, W. Yu, L. Gao, D. Shi, J. Ju, N. Deng, W. Kang, *Energy Storage Mater.* **2023**, *63*, 103005.
[33] M.-C. Long, T. Wang, P.-H. Duan, Y. Gao, X.-L. Wang, G. Wu, Y.-Z. Wang, *J. Energy Chem.* **2022**, *65*, 9–18.
[34] C. Guo, Y. Cao, J. Li, H. Li, S. Kumar Arumugam, S. Oleksandr, F. Chen, *Appl. Energy* **2022**, *323*, 119571.
[35] L. Y. Chou, Y. Ye, H. K. Lee, W. Huang, R. Xu, X. Gao, R. Chen, F. Wu, C. K. Tsung, Y. Cui, *Nano Lett.* **2021**, *21*, 2074–2080.
[36] C. Fu, G. Homann, R. Grissa, D. Rentsch, W. Zhao, T. Gouveia, A. Falgayrat, R. Lin, S. Fantini, C. Battaglia, *Adv. Energy Mater.* **2022**, *12*, 2200412.
[37] Z. Tian, L. Hou, D. Feng, Y. Jiao, P. Wu, *ACS Nano* **2023**, *17*, 3786–3796.
[38] J.-S. Park, C.-H. Jo, S.-T. Myung, *Energy Storage Mater.* **2023**, *61*, 102869.
[39] Y. Huang, S. Liu, Q. Chen, K. Jiao, B. Ding, J. Yan, *Adv. Funct. Mater.* **2022**, *32*, 2201496.
[40] Y. Cui, J. Wan, Y. Ye, K. Liu, L.-Y. Chou, Y. Cui, *Nano Lett.* **2020**, *20*, 1686–1692.
[41] Y. Wang, L. Wu, Z. Lin, M. Tang, P. Ding, X. Guo, Z. Zhang, S. Liu, B. Wang, X. Yin, Z. Chen, K. Amine, H. Yu, *Nano Energy* **2022**, *96*, 107105.
[42] W. Bao, L. Zhao, H. Zhao, L. Su, X. Cai, B. Yi, Y. Zhang, J. Xie, *Energy Storage Mater.* **2021**, *43*, 258–265.
[43] J. Zhang, Y. Zeng, Q. Li, Z. Tang, D. Sun, D. Huang, L. Zhao, Y. Tang, H. Wang, *Energy Storage Mater.* **2023**, *54*, 440–449.
[44] H. Yang, B. Zhang, M. Jing, X. Shen, L. Wang, H. Xu, X. Yan, X. He, *Adv. Energy Mater.* **2022**, *12*, 2201762.
[45] H. Kim, U. H. Yoon, T. I. Ryu, H. J. Jeong, S. il Kim, J. Park, Y. S. Kye, S.-R. Hwang, D. Kim, Y. cho, K. Jeong, *New J. Chem.* **2022**, *46*, 8653–8661.
[46] Y. Zhu, Y. Shi, Z.-Q. Huang, L. Duan, Q. Tai, Y. Hu, *Composites Part A: Applied Science and Manufacturing* **2017**, *99*, 149–156.
[47] Z. Wang, J. Sun, R. Liu, Z. Ba, J. Dong, Q. Zhang, X. Zhao, *Small* **2023**, *19*, 2303422.

Manuscript received: January 31, 2024
Revised manuscript received: April 11, 2024
Accepted manuscript online: April 12, 2024
Version of record online: May 8, 2024